ARTICLE

www.the-innovation.org

Radiative trigger thresholds of foliar photoprotective pigment regulation for global vegetation

Wenjin Wu,[1,2,3] Howard Epstein,[4] Xiyan Xu,[5] Xinwu Li,[1,2,*] Huadong Guo,[1,2,*] and Jinfeng Li[6]

*Correspondence: lixw@aircas.ac.cn (X.L.); guohd@aircas.ac.cn (H.G.)

Received: October 17, 2023; Accepted: May 23, 2024; Published Online: May 24, 2024; https://doi.org/10.1016/j.xinn.2024.100649

GRAPHICAL ABSTRACT

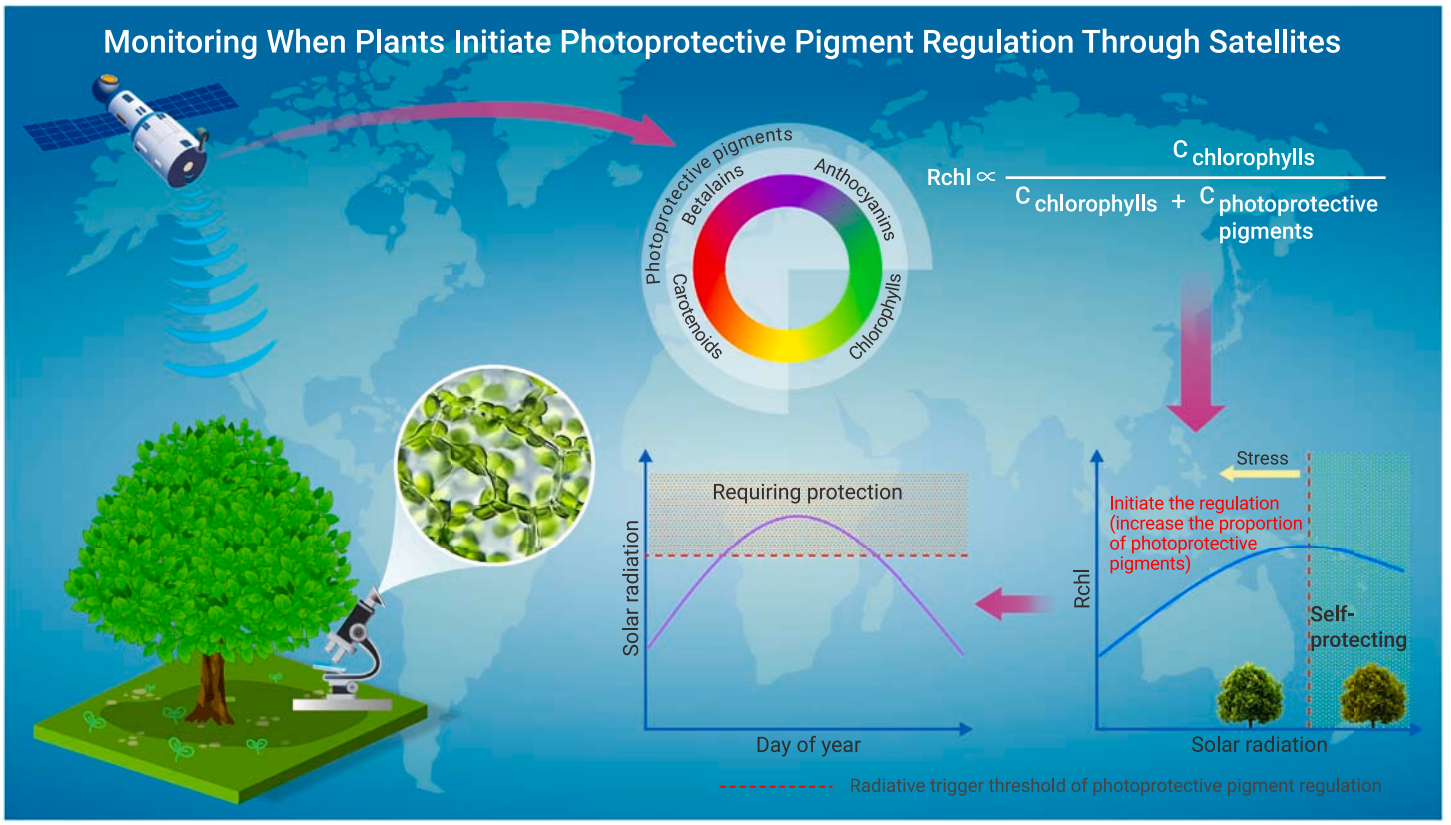

PUBLIC SUMMARY

- Foliar photoprotective pigmental adjustment is a common long-term self-protection mechanism for global vegetation.
- A remote sensing method is proposed to monitor abiotic stress by detecting when plants initiate such protection.
- A high-stress zone around 60°N is identified and predicted to shift southward in the future.
- Warming will reduce radiation tolerance and increase the risk of photodamage for plants in northern high latitudes.

ARTICLE

Radiative trigger thresholds of foliar photoprotective pigment regulation for global vegetation

Wenjin Wu,[1,2,3] Howard Epstein,[4] Xiyan Xu,[5] Xinwu Li,[1,2,*] Huadong Guo,[1,2,*] and Jinfeng Li[6]

[1]International Research Center of Big Data for Sustainable Development Goals, Beijing 100094, China

[2]Key Laboratory of Digital Earth Sciences, Aerospace Information Research Institute, Chinese Academy of Sciences, Beijing 100094, China

[3]Key Laboratory of Earth Observation of Hainan Province, Hainan Research Institute, Aerospace Information Research Institute, Chinese Academy of Sciences, Sanya 572029, China

[4]Department of Environmental Sciences, University of Virginia, Charlottesville, VA, USA

[5]Key Laboratory of Regional Climate-Environment for Temperate East Asia, Institute of Atmospheric Physics, Chinese Academy of Sciences, Beijing 100029, China

[6]State Key Laboratory of Plant Diversity and Specialty Crops, Institute of Botany, Chinese Academy of Sciences, Beijing 100093, China

*Correspondence: lixw@aircas.ac.cn (X.L.); guohd@aircas.ac.cn (H.G.)

Received: October 17, 2023; Accepted: May 23, 2024; Published Online: May 24, 2024; https://doi.org/10.1016/j.xinn.2024.100649

Citation: Wu W., Epstein H., Xu X., et al., (2024). Radiative trigger thresholds of foliar photoprotective pigment regulation for global vegetation. The Innovation **5(4)**, 100649.

Adjustments in foliar photoprotective pigments are crucial for plant adaptation to harsh environments, serving as indicators of environmental stress. However, understanding when and where these adjustments occur across diverse biomes remains unclear due to challenges in large-scale observation. Here, we propose a novel approach to assess dynamics in photoprotective pigments at the canopy level using a new index derived from space-borne optical sensors. This approach generates a global map depicting the daily mean shortwave radiation threshold at which adjustments typically occur under prevailing climatic conditions. The global average of this threshold is 262 ± 50 W m^{-2}, with lower values at high latitudes and peaks near 40° in both hemispheres. Temperature exerts a stronger influence on this latitudinal pattern than humidity. Future projections suggest a decrease in this threshold over northern high latitudes, implying exacerbated vulnerability under identical radiation levels due to negative warming responses. Based on this threshold, a high-stress zone around 60°N is identified and is predicted to shift southward in the future. These findings bridge critical gaps in photoprotection research and offer a new perspective on understanding the biogeochemical cycles of global ecosystems. This framework can also enhance our ability to predict the fate of diverse ecosystems under future climate.

INTRODUCTION

Land plants play a vital role in sustaining life on Earth by producing oxygen, supplying food, and creating habitats.[1] Understanding their biochemical responses and susceptibility to climate change is essential for achieving global sustainable development goals.[2,3] In adapting to challenging environments, plants have evolved diverse self-protection mechanisms,[4,5] greatly promoting their resilience and survivability in the future climate. Among them, the foliar photoprotective pigment regulation (PP) through increasing the proportions of photoprotective pigments in the canopy is a common long-term environmental coping strategy.[6,7] These photoprotective pigments fall into three major groups: carotenoids, anthocyanins, and betalains.[4,6] PP can thus be monitored using the ratio of foliar chlorophylls to the sum of chlorophylls and the aforementioned photoprotective pigments,[8] termed as the chlorophyll ratio:

$$\text{chlorophyll ratio} = \frac{C_{chl}}{C_{chl}+C_{pp}}, \qquad \text{(Equation 1)}$$

where C_{chl} and C_{pp} denote contents of chlorophylls and foliar photoprotective pigments (μg cm^{-2}), respectively.

PP provides an indication of when plants "feel stressed" and are self-protecting. As a mechanism to safeguard the photosynthetic reaction center, PP is directly triggered in response to excessive radiation[9-11] that can cause photodamage and plant mortality.[12,13] With this mechanism in place, the foliar chlorophyll ratio, which typically increases with radiation to take full advantage of light,[14] decreases upon reaching a threshold (PPtrigger) due to the activation of PP.[15,16] This process typically takes days and should be distinguished from rapidly reversible de-epoxidation reactions that adjust light partitioning without altering the pigment pool. Other stressors such as drought, frost, and nutrient deficiency can diminish plant resistance to intense irradiance,[17-21] leading to a reduced PPtrigger (Figure 1). Therefore, PPtrigger serves as a comprehensive index that can be used to examine if the overall environmental conditions are suitable for vegetation growth.[22] We define PPratio as the proportion of days in the growing season per year when the radiation level exceeds PPtrigger. It can thus reflect how adverse the environment is to vegetation growth, i.e., a higher PPratio indicates a longer period of stress.

Due to the absence of space-borne methods, earlier investigations on PP have exclusively depended on field measurements.[23-25] This hindered the understanding of PP on a large scale. To address this problem, we introduced a new remotely sensed index, Rchl,[13] to upscale the analysis of chlorophyll ratios across global vegetation. Rchl utilizes reflectance around 520 nm, where carotenoids and anthocyanins have similar absorption rates, and near 675 nm, where reflectance is primarily determined by the content of chlorophylls, to estimate the chlorophyll ratio[7]:

$$\text{Rchl} = \frac{\text{GREEN}_{520nm}}{\text{GREEN}_{520nm}+\text{RED}_{675nm}} \approx \frac{\rho_{11}}{\rho_{11}+\rho_{13}}, \qquad \text{(Equation 2)}$$

where GREEN_{520nm} and RED_{675nm} are the reflectance at 520 and 675 nm, respectively, which can be derived from the reflectance (ρ_x) in band x of the Moderate Resolution Imaging Spectroradiometer (MODIS). Although originally designed to target carotenoids and anthocyanins, considering that betalains have similar spectral properties to anthocyanins,[6] Rchl should also consider betalains. This suggests that Rchl has the potential to encompass all major types of photoprotective pigments in vegetation, which differs from existing remotely sensed vegetation indices.[26] We propose a method to assess the spatiotemporal distribution of PPtrigger and PPratio with Rchl. PPtrigger is estimated through the local-maxima detection using smoothed Rchl-radiation curves. For the radiation metric, we use the daily mean shortwave radiation (SWR) considering the timescale of PP.

Using global Rchl series over 2001–2020, we, for the first time, present a global map of PPtrigger under prevailing environmental conditions, responses of PPtrigger to heat and moisture for different ecosystems, and the general stress level estimated by PPratio under current and future scenarios. We address a crucial scientific question for climate change, ecophysiology, and Earth system modeling communities: how does PP vary across different biomes globally and in response to environmental factors? The findings reveal suitable environments and the current and future stress levels for various terrestrial ecosystems.

RESULTS

The global distribution of PPtrigger under prevailing environmental conditions

We initially plotted Rchl-SWR relationships for 161 FLUXNET sites[27] along with the corresponding leaf area index (LAI), gross primary production (GPP), and net ecosystem production (NEP). Results from two northern grassland sites (NL-Hor and CZ-BK2) located at similar latitudes are displayed as examples (Figure 2). At both sites, vegetation growth peaks around the summer solstice when solar irradiance is at the maximum. These synchronized growth and radiation peaks minimize any underlying phenological effects on PPtrigger estimations. At NL-Hor, the relationship exhibits an inflection point in Rchl with respect to SWR indicating

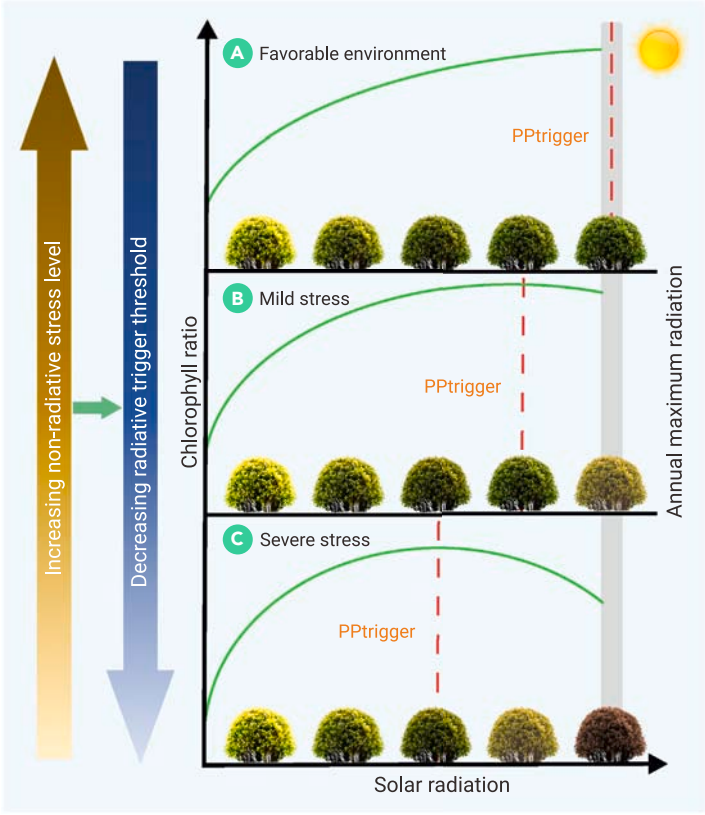

Figure 1. The conceptual framework showing how PPtrigger responds to environmental stress and affects plant growth Green curves display relationships between radiation and the chlorophyll ratio. Plant status is depicted by its color, while PPtrigger is highlighted with a red dotted line in each case. In (A), PP is not triggered because the radiation level is below the trigger threshold. In (B), the plant's tolerance to radiation decreases (PPtrigger decreases) due to abiotic stress.[16-21] PP is triggered earlier than in (A), effectively safeguarding the photosynthetic system. In (C), the plant's tolerance to radiation significantly diminishes due to severe stress (PPtrigger further decreases). Despite PP being triggered even earlier than in (B), its protective capacity is insufficient to safeguard the photosynthetic center. Photodamage occurs, leading to reduced productivity and, potentially, the plant's failure to survive.[13]

PP and identifying PPtrigger. Conversely, at CZ-BK2, Rchl increases with SWR continuously, which indicates that PP is not triggered, and PPtrigger is undetected. For reference, the LAI at both sites increases monotonically with SWR, and productivity does not significantly decrease at high SWR levels. This suggests that when SWR exceeds PPtrigger, the decline of Rchl is not attributed to biomass loss or cessation of plant growth. Therefore, the inflection point in the Rchl-SWR curve is associated with the activation of PP. Rchl-SWR relationships for several other biomes are displayed in Figure S4.

Based on SWR and Rchl data in 2001–2020, the average PPtrigger of global vegetation was estimated to be 262 ± 50 W m^{-2} (mean ± 1 SD) (Figure 3). This corresponds to ~118 ± 23 W m^{-2} in photosynthetically active radiation or ~543 ± 106 μmol m^{-2} s^{-1} in photosynthetic photon flux density (PPFD).[28] Over the two decades, PPtrigger was detected in 56% of the vegetated surface, indicating widespread environmental stress. The remaining areas are mainly located in the tropics, where temperature and moisture conditions are generally favorable for vegetation growth. There could be two cases in which PPtrigger is not detected. First, when the environmental radiation is lower than PPtrigger, PP remains inactive throughout the study period. Second, some plant species lack the ability to synthesize photoprotective pigments in the canopy and utilize alternative photoprotection strategies such as altering leaf orientation and producing wax layers.[29] Although tropical regions may experience the strongest annual mean SWR, due to the even distribution of radiation throughout the year, the annual maximum radiation is lower compared to middle latitudes as shown in on the right in Figure 3. The first case could possibly be an explanation for the absence of PPtrigger detection. Low PPtrigger values (~150–220 W m^{-2}) are mainly found in cold regions, including northern Europe and northeast Canada, where plants reach photosaturation at reduced radiation levels under low temperatures.[30] High PPtrigger values (>300 W m^{-2}) are scattered across the subtropics of both hemispheres, with greater distribution in the Southern Hemisphere. This pattern may correspond to the dominance of C_4 plants, which are well adapted to high levels of light.[31]

The latitudinal average of PPtrigger has essentially a hemispheric symmetry (Figure 3). Regions around 60°N and 60°S show the highest percentage of pixels with observed PPtrigger, while those at approximately 40°N and 40°S show the highest PPtrigger values coinciding with large annual maximum SWR. Southern Hemisphere regions generally display greater PPtrigger values compared to mirror latitudes in the north. This is consistent with greater maximum insolation in the Southern Hemisphere (by ~6.9%) than in the north,[32] reflecting the adaptation of plants to their respective environments. Influenced by topography, the annual maximum SWR over the Tibetan Plateau, the world's highest plateau, is 369 W m^{-2}, which is comparable to that over 40°S and higher than that over 40°N. Areas above the Arctic Circle exhibit the largest differences between PPtrigger and annual maximum SWR, implying a high need for photoprotection. This explains the prevalence of reddish leaves[33,34] and low chlorophyll ratios (Figure S5) in Arctic vegetation. It also underscores the importance of accurately mapping the photoprotection capacity and photodamage risks over northern high latitudes.

The statistical results for different biomes reveal distinct patterns in PPtrigger (Figures S6 and S7). Herbaceous plants in grass-dominated savannas and grasslands generally exhibit higher PPtrigger values compared to woody plants. Within the woody category, evergreens display even lower PPtrigger values because evergreen species in challenging environments tend to maintain higher levels of photoprotective pigments to ensure their long-term survival.[35,36] Permanent wetland ecosystems have the lowest PPtrigger due to unique soil properties, such as saline or frozen conditions, which often challenge vegetation growth. Wetlands can also host mosses and lichens, which possess non-green pigments[37,38] similar to PP in vascular plants. These findings highlight the diversity of photoprotection strategies adopted by different vegetation types.

Responses of PPtrigger to climate variations

Modulations in environmental stress can induce changes in PPtrigger (see an example in Figure S8). To model the temporal relationships between PPtrigger and climate conditions, we conducted a partial least squares (PLS) regression analysis,[39] regressing PPtrigger against two crucial environmental factors,[39] air temperature and soil moisture (see materials and methods). 310 out of 597 ecoregions demonstrate significant correlations ($p < 0.05$) with R = 0.45 ± 0.18 (mean ± 1 SD). The unexplained portion of PPtrigger variation may be attributed to dynamic soil nutrition and unconsidered climatic factors such as daily temperature fluctuations and wind.

Responses of PPtrigger to heat and moisture vary largely across different regions and biomes (Figure 4). Impacts of temperature are generally greater than moisture, indicating the dominance of heat status effects on PPtrigger. Most regions near 60°N and 60°S show positive responses of PPtrigger to temperature since the primary stress in this region is cold stress. Under the current warming trend, PPtrigger will increase, thereby reducing the risk of photodamage under equivalent radiation. In northern Canada, Alaska, northern Russia, and Mongolia, PPtrigger exhibits negative responses to both temperature and soil moisture, suggesting decreased radiation tolerance in hot and wet climates. On the Tibetan Plateau, PPtrigger shows a pronounced negative response to temperature and a positive response to moisture, indicating susceptibility to heat and drought stress.[40] PPtrigger of most tree types responds positively to temperature, maintaining its competitive advantage in a warming climate. Conversely, the responses are negative for closed shrubland, indicating detrimental effects of warming (Figure S9).

PPratio in current and future scenarios

With current conditions, 37% of vegetated areas are under stress during the growing season, and the global mean PPratio is estimated to be 0.094 (Table S1). The proportion of days requiring PP in the Northern Hemisphere is generally larger than that in the Southern Hemisphere (Figure 5A). Compared with North America, Eurasia displays a higher PPratio, which can even reach the half of the growing season near 60°N. Among different biomes, evergreen needleleaf forest and permanent wetland show the greatest PPratio, while most evergreen broadleaf forest and savanna regions exhibit PPratios of zero

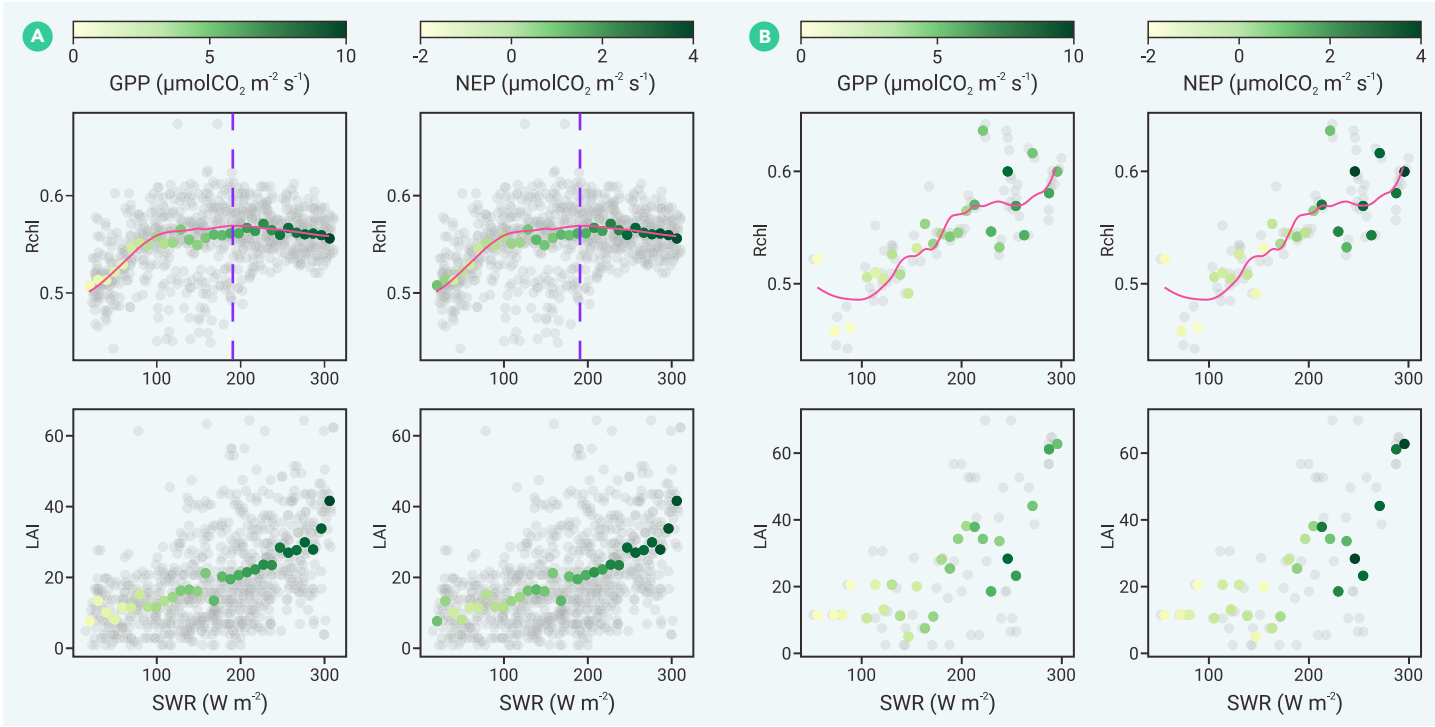

Figure 2. Examples of PPtrigger estimation (A) Site NL-Hor (52.24°N, 5.07°W, temperate grassland, 2004–2011). (B) Site CZ-BK2 (49.49°N, 18.54°E, alpine grassland, 2004–2006). Gray points represent the original scatter points of Rchl-SWR and LAI-SWR. Colored points denote the binned vegetation index values according to SWR, where variations caused by other factors are suppressed. Point colors on the left and right correspond to GPP and NEP values, respectively. Pink lines show smoothed Rchl-SWR curves, with purple dotted lines highlighting the PPtrigger estimations.

(Figure S7). Therefore, PP is of different importance among various vegetation types.

To quantify the influence of PPtrigger changes, PPratio for the end of the 21st century was predicted under a moderate forcing scenario (SSP2-4.5) and a high-end forcing scenario (SSP5-8.5). The projection was performed for areas with detected PPtrigger under two assumptions. The static assumption assumes no acclimation of PPtrigger over time, while the dynamic assumption considers possible acclimation of PPtrigger over time (see materials and methods).

Under the static assumption, the total area of vegetation with positive PPratio decreases from 37% to 25% (26%) under SSP2-4.5 (SSP5-8.5) (Figures 5B and 5D). This indicates that radiation constraints are eliminated in approximately one-third of the currently stressed area (Table S1). A shift of the high-PPratio zone from ~60°N to 30°–50°N occurs in both scenarios due to a change in radiation,[41] which portends elevated environmental stress for mid-latitude vegetation. Compared to SSP2-4.5, SSP5-8.5 shows a similar trend of decreases in PPratio, with larger decreases around 60°N. Tropical ecosystems will remain in their current state with minimal PPratio. Grasslands and croplands show increased PPratios due to a change in radiation level (Figure S6B), which raises concerns about their reduced competitiveness and productivity.

Under the dynamic assumption, increases in PPratio due to reduced PPtrigger (Figure 5F) are found over northern high latitudes, middle latitudes of Eurasia, the West Coast of the United States, and northern Argentina (Figures 5C and 5E). Extra threats of photodamage in northern high latitudes warrant particular attention, where PPtrigger responds negatively to temperature and the warming is much greater than elsewhere on Earth.[42] Compared with results under the static assumption, an increase in PPratio (+4.70% under SSP2-4.5 and +2.71% under

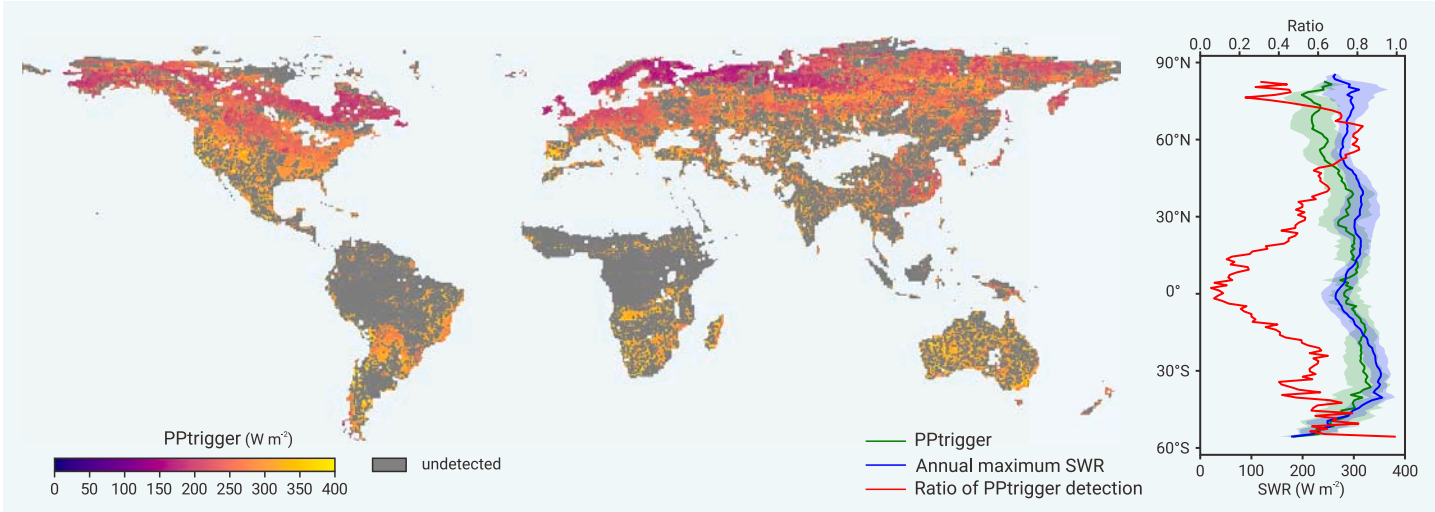

Figure 3. PPtrigger of global vegetation The map was generated using smoothed Rchl-SWR curves in 2001–2020. The line and shaded area in the line chart represent the mean and standard deviation for PPtrigger, annual maximum SWR, and the ratio of PPtrigger detection, summarized for each 1° latitudinal zone.

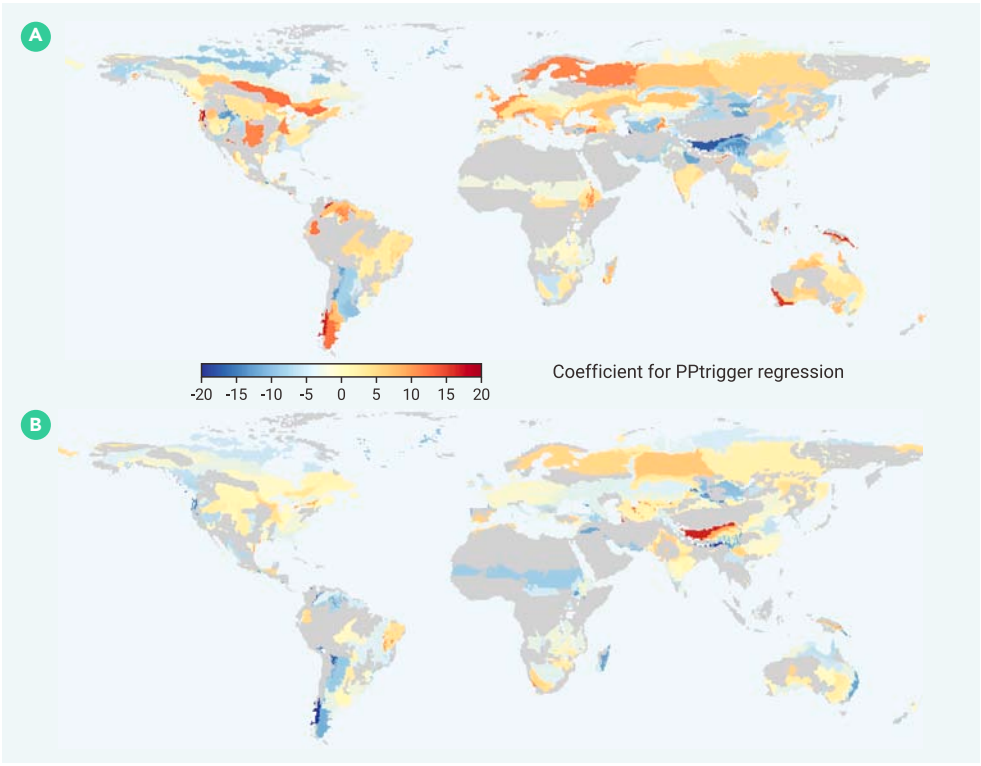

Figure 4. Responses of PPtrigger to non-radiative climatic variables Responses of PPtrigger to temperature (A) and soil moisture (B). Results were derived for each ecoregion using normalized variables indicating the relative impact strength. Only significant results ($p < 0.05$) are presented.

SSP5-8.5) is also projected, demonstrating that the benefits of more conducive future radiation will be partially offset.

DISCUSSION

Relationships between PPtrigger and the light saturation point of photosynthesis

PP is a long-term mechanism, and the accumulation of photoprotective pigments is triggered by prevailing excessive radiation. Therefore, in this study, we opted for a diurnal mean radiation metric for PPtrigger. In contrast, de-epoxidation reactions are triggered when radiation suddenly surpasses the light saturation point of photosynthesis.[43] With regard to PPFD, C_4 species exhibit a light saturation point of 1,200–1,600 μmol m^{-2} s^{-1}, whereas this value peaks at approximately 800 μmol m^{-2} s^{-1} in C_3 plants at the stand level.[9] These values correspond to 580–773 and 387 W m^{-2} in SWR, which is about twice our estimation of globally averaged PPtrigger (262 ± 50 W m^{-2}). PPFD is an instantaneous radiation comparable to the radiation around noon, which is possibly twice the daily mean. Thus, our results are comparable to the light saturation point of photosynthesis derived from *in situ* experiments, although they are not necessarily identical.

Relationships between PP and productivity

Previous studies reported benefits of high foliar photoprotective pigment concentrations in maintaining photosynthesis rates under environmental stress.[17,21] To evaluate relationships between PP and productivity, we assessed daily CO_2 flux measurements from 100 eddy covariance sites where PPtrigger was detected. Flux data were aligned based on the difference between their corresponding SWR and PPtrigger values to ensure a consistent stress level across different sites. The aligned data were binned and averaged to minimize productivity variations caused by other factors. The results show that PP allows both GPP and NEP to be maintained with minimal declines (<7% of the maximum reduction) until SWR exceeds PPtrigger by up to ~59 W m^{-2} on average, which reveals the capacity limit of PP (Figure S10). As SWR continues to increase above this limit, GPP and NEP decrease linearly at 0.0145 (R^2 = 0.87, $p < 0.01$) and 0.0078 μmol CO_2 s^{-1} W^{-1} (R^2 = 0.78, $p < 0.01$), leading to productivity reductions of up to 58% and 34%, respectively. This indicates that with the photoprotection provided by PP, productivity can be largely sustained unless the stress surpasses the capacity limit of PP.

Comparisons between Rchl and existing vegetation indices in PP monitoring

To further elucidate the performance of Rchl in PP monitoring, we compared the ability of Rchl to track the dynamics of chlorophyll ratios with three widely used indices: the normalized difference vegetation index (NDVI), the enhanced vegetation index (EVI), and the chlorophyll carotenoid index (CCI)[44] (Figure S11). The spectral data utilized in this analysis were generated using the PROSAIL-D radiative transfer model,[45] accounting for varying LAIs and compositions of the canopy pigment pool. All vegetation indices were computed based on the broadband reflectance of MODIS. NDVI and EVI tend to saturate when the chlorophyll ratio is approximately 0.6. This value falls within the median chlorophyll ratio of living vegetation (Figure S2), suggesting that these two indices are not sensitive enough to capture the full internal dynamics of the foliar pigment pool. CCI has a higher saturation point, approximately around 0.7, yet its relationship with the chlorophyll ratio is non-linear. In contrast, Rchl demonstrates a consistent linear relationship with the chlorophyll ratio, indicating its robust capability for PP monitoring.

Uncertainties and limitations in PPtrigger predictions

The response of PP to strong irradiance is regulated by many abiotic factors, implying that PPtrigger may vary throughout different periods within a year. To capture a general temporal trend, short-term fluctuations were minimized through multi-year data binning in this study, which also mitigates errors in the PPtrigger estimation caused by uncertainties in the Rchl (e.g., directional effects). Limited by data availability and computation ability, we only considered air temperature and soil moisture variations in future projections, while other factors such as soil nutrients, wind, and species replacement may also influence PPtrigger and PPratio. Additionally, short-statured plants can benefit from radiative heating of the soil, leading to differences between foliage and air temperatures, which might introduce complexities in regression analysis. These issues may all contribute to uncertainties in PPtrigger predictions. Future studies necessitate increased field observations worldwide, longer series of remote sensing data, and further development of ecosystem models to solve these issues.

CONCLUSION

Employing a newly developed remote sensing method, we conducted an inaugural global analysis of foliar PP in vegetated areas. The globally averaged PPtrigger value of 262 ± 50 W m^{-2} aligns with ecophysiological knowledge and field observation statistics. By utilizing the triggering condition of this mechanism, we reveal the stress levels experienced by plants across diverse ecosystems under current and future climate scenarios. Our findings emphasize a high-stress zone around 60°N, with a projected shift toward lower latitudes in the future. Moreover, the potential exacerbation of stress in northern high latitudes (70°–80°N) due to reductions in radiation tolerance triggered by warming is also highlighted. These discoveries will not only enhance our understanding of ecosystem resilience but also support improvements of biogeochemical simulations in ecological models. The potential usefulness of PPtrigger and PPratio in predicting plant survivability also underscores their significance in forecasting vegetation distribution in Earth system models.

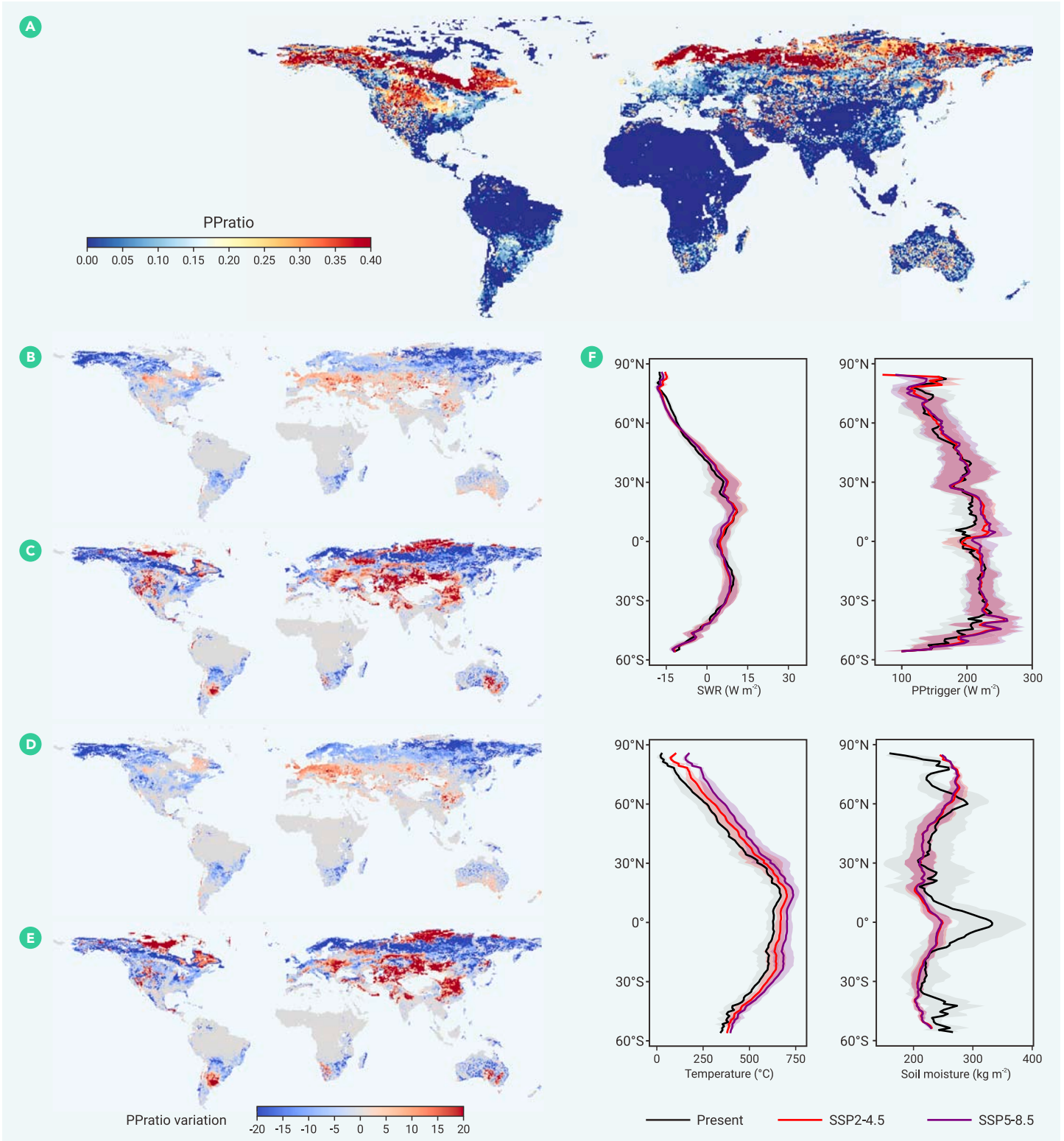

Figure 5. Present (2011–2020) and future (2091–2100) PPratio of global vegetation (A) Present PPratio. (B and C) Change of PPratio under SSP2-4.5 using the static and dynamic assumptions. (D and E) Change of PPratio under SSP5-8.5 using the static and dynamic assumptions. (F) Latitudinal distribution of present and future SWR, PPtrigger, temperature, and soil moisture, where curves and their shaded areas indicate the mean and standard deviation summarized over vegetated areas within each 1° latitudinal zone.

MATERIALS AND METHODS

Rchl validation and calculation

Rchl is a spectral index used to approximate the chlorophyll ratio using satellite data. Validated with real and simulated data (Figures S1–S3), the index is not significantly affected by variations in species, LAI, solar zenith angles, and viewing zenith angles, which allows us to map PPtrigger globally. To derive Rchl, we utilized surface reflectance data obtained from the daily MODIS products MODOCGA[46] and MYDOCGA.[47] For eddy covariance sites, we obtained daily Rchl series at 1 km resolution during 2001–2020. For spatially continuous global time series, we initially obtained 8 day Rchl medians and then averaged the values in each month over 2001–2020 at a spatial resolution of 0.5°.

Productivity data

Daily GPP and NEP (μmol CO_2 m^{-2} s^{-1}) at eddy covariance sites were extracted from the FLUXNET2015 dataset,[27] which comprises 165 sites covering major vegetation types

worldwide and provides *in situ* productivity records. NEP data were approximated as the negative value of the net ecosystem exchange. Four sites were excluded due to insufficient matching Rchl or climatic variable records during the growing season, leaving 161 sites in the analysis (Figure S6).

NDVI, EVI, and LAI data

NDVI and EVI were calculated based on MODIS daily surface reflectance.[46,47] LAI was acquired from the MODIS products MOD15A2H and MYD15A2H[48] to ensure an optimal consistency in spatiotemporal cover and quality with Rchl, thereby facilitating an effective delineation of the contrasting behaviors between Rchl and LAI.

Climate data

Three climatic variables including SWR (W m^{-2}), air temperature (°C), and soil moisture (kg m^{-2}) were used in this study, which are crucial for vegetation growth.[49] During 2001–2020, we generated data from the v.2.1 dataset of the Global Land Data Assimilation System (GLDAS)[50] with an original spatial resolution of 0.25° and a temporal frequency of 3 h. Daily time series data for each variable were generated and resampled to match the spatial grids of the eddy covariance sites as well as the global Rchl maps.

For future climate projections, we adopted ensembled variable values from 23 models in the sixth phase of the Coupled Model Intercomparison Project (CMIP6)[51] for 2091–2100. Two scenarios were considered: SSP2-4.5 and SSP5-8.5.[52] To match the climatic variables used in the current condition, the surface downwelling shortwave flux (rsds), 2 m near surface air temperature (tas), and total soil moisture content (mrso) were selected. 133 simulation outputs containing all the aforementioned variables were included in the ensemble (Table S2). To address any inconsistency between GLDAS and CMIP6 outputs, we transformed the future climate data into GLDAS-equivalent data based on relationships calculated from their overlapping period (2015–2020) (Figure S12). Daily time series for the three variables were then calculated and averaged over 2091–2100 and resampled to a 0.5° resolution (Figure S13).

Vegetation distribution maps

To identify vegetation functional types, we used the map produced by the International Geosphere-Biosphere Programme[53] (Figure S6). The terrestrial ecoregion map published by the World Wildlife Fund[54] was employed to support the regression of PPtrigger. Ecosystems within each ecoregion were assumed to have similar type, quality, and quantity of biotic components as well as environmental resources. Therefore, we presumed a uniform equation within each ecoregion in the regression.

PPtrigger estimation

PPtrigger was estimated with an inflection point detection method based on smoothed Rchl-SWR curves. The Rchl-SWR points during the growing season over 2001–2020 were first aggregated into small bins using the median value to suppress short-term variations caused by varying meteorological conditions or temporal disturbance events. The growing season was defined as the period characterized by NDVI ≥ 0.1 and a daily mean temperature threshold of 0°C considering the polar regions within our study area.[55] This masking also removed snow-contaminated data, which could introduce uncertainties in Rchl and bias the inflection point detection. The scatter points were then smoothed using a 3° Savitzky-Golay filter[56] and interpolated with the quadratic B-spline method[57] to ensure a consistent SWR step of 1 W m^{-2} across different locations. Local maxima of each curve were detected, and those with SWR ≤ 100 W m^{-2} were removed, as this radiation level is unlikely excessive for plants. Among the rest of the local maxima, the one with the maximum Rchl was retained as the candidate trigger point for PP. Trends for Rchl changes on both sides of that point were further checked to determine whether it is a true trigger point or not. If no trigger point was found, then PPtrigger would be marked as undetected.

We applied the method separately to daily and monthly Rchl-SWR data from 161 eddy covariance sites. A strong linear correlation was found between the two results (Pearson's $r = 0.77$, $p < 0.001$, Figure S13). We then used this relationship to convert the global PPtrigger map obtained from monthly series and support the PPratio calculation based on daily SWR.

PLS regression

PLS regression is a method used to establish a linear relationship between predicted and observable variables, especially when multiple independent variables are coupled.[37] We employed this method to model the relationships between PPtrigger and core climatic variables (mean air temperature and soil moisture). Within each ecoregion, we extracted PPtrigger from each 0.5° grid cell using a 5 year temporal sliding window and derived the corresponding climatic variables. Only ecoregions with more than 20 valid samples were retained, and the samples were then split into two groups, with 70% used for training and 30% for validation. Climatic variables were standardized for comparisons of their levels of impact on PPtrigger variations. Results were considered to be significant when $p < 0.05$ for Pearson's correlation between the predicted and observed variables.

PPratio computation

To obtain PPratio, the number of days during the growing season when daily mean SWR exceeds PPtrigger is first determined, which is then divided by the total length of the growing season in a year. We used 2011–2020 for a current scenario and 2091–2100 for future projections. To project PPtrigger values in future scenarios, we recalculated PPtrigger for ecoregions that exhibited significant responses to climate change. This was achieved by inputting future temperature and soil moisture data under SSP2-4.5 and SSP5-8.5 into the previously derived PLS equations. Note that this process may increase the homogeneity and reduce the dynamic range of PPtrigger within each ecoregion. However, this should not significantly impact statistics averaged over latitudinal zones or vegetation types.

REFERENCES

1. Foley, J.A., Defries, R., Asner, G.P., et al. (2005). Global consequences of land use. Science ***309***(5734): 570–574. https://doi.org/10.1126/science.1111772.
2. Freedman, B. (2009). Environmental Science (Pearson Education Canada), p. 15.
3. Zhang, X., Liu, J., Zeng, J., et al. (2024). Impact of drought-induced forest mortality on terrestrial carbon cycle from remote sensing perspective. The Innovation Geosci. ***2***(1): 100057. https://doi.org/10.59717/j.xinn-geo.2024.100057.
4. Solovchenko, A. (2010). Photoprotection in Plants, Optical Screening-Based Mechanisms (Springer Science & Business Media), p. 14.
5. Pinnola, A., and Bassi, R. (2018). Molecular mechanisms involved in plant photoprotection. Biochem. Soc. Trans. ***46***(2): 467–482. https://doi.org/10.1042/BST20170307.
6. Solovchenko, A.E., and Merzlyak, M.N. (2008). Screening of visible and UV radiation as a photoprotective mechanism in plants. Russ. J. Plant Physiol. ***55***(6): 719–737. https://doi.org/10.1134/S1021443708060010.
7. Gitelson, A.A., Keydan, G.P., and Merzlyak, M.N. (2006). Three-band model for noninvasive estimation of chlorophyll, carotenoids, and anthocyanin contents in higher plant leaves. Geophys. Res. Lett. ***33***(11): L11402. https://doi.org/10.1029/2006GL026457.
8. Gamon, J.A., and Surfus, J.S. (1999). Assessing leaf pigment content and activity with a reflectometer. New Phytol. ***143***(1): 105–117. https://doi.org/10.1046/j.1469-8137.1999.00424.x.
9. Santos, M., Ferreira, E., Valadão, D., et al. (2017). Brachiaria physiological parameters in agroforestry systems. Ciência Rural. ***47***(5): e20160150. https://doi.org/10.1590/0103-8478cr20160150.
10. Phuong, N., and Valeriano, C. (2009). The role of light on foliage colour development in coleus (Solenostemon scutellarioides (L.) Codd). Plant Physiol. Biochem. ***47***(10): 934–945. https://doi.org/10.1016/j.plaphy.2009.06.006.
11. Stetsenko, L., Pashkovsky, P., Voloshin, R., et al. (2020). Role of anthocyanin and carotenoids in the adaptation of the photosynthetic apparatus of purple- and green-leaved cultivars of sweet basil (Ocimum basilicum) to high-intensity light. Photosynthetica ***58***(4): 890–901. https://doi.org/10.32615/ps.2020.048.
12. Wang, Y., Xia, A., and Xue, K. (2024). Cold and humid climates enrich soil carbon stock in the Third Pole grasslands. Innovation ***5***(1): 100545. https://doi.org/10.1016/j.xinn.2023.100545.
13. Alonso, Z., and Cristian, M. (2021). Concepts of photochemical damage of Photosystem II and the role of excessive excitation. J. Photoch. Photobio. ***47***: 100421. https://doi.org/10.1016/j.jphotochemrev.2021.100421.
14. Wu, W., Epstein, H.E., Guo, H., et al. (2021). A pigment ratio index based on remotely sensed reflectance provides the potential for universal gross primary production estimation. Environ. Res. Lett. ***16***(5): 054065. https://doi.org/10.1088/1748-9326/abf3dc.
15. Lee, D.W. (2002). Anthocyanins in leaves: Distribution, phylogeny and development. Adv. Bot. Res. ***37***: 37–53. https://doi.org/10.1016/S0065-2296(02)37042-3.
16. Galmés, J., Abadía, A., Medrano, H., et al. (2007). Photosynthesis and photoprotection responses to water stress in the wild-extinct plant Lysimachia minoricensis. Environ. Exp. Bot. ***60***(3): 308–317. https://doi.org/10.1016/j.envexpbot.2006.12.016.
17. Oberbaueri, S.F., and Starr, G. (2002). The role of anthocyanins for photosynthesis of Alaskan arctic evergreens during snowmelt. Adv. Bot. Res. ***37***: 129–145. https://doi.org/10.1016/S0065-2296(02)37047-2.
18. Hughes, N.M., Reinhardt, K., Feild, T.S., et al. (2010). Association between winter anthocyanin production and drought stress in angiosperm evergreen species. J. Exp. Bot. ***61***(6): 1699–1709. https://doi.org/10.1093/jxb/erq042.
19. Murata, N., Takahashi, S., Nishiyama, Y., et al. (2007). Photoinhibition of photosystem II under environmental stress. Biochim. Biophys. Acta. ***1767***(6): 414–421. https://doi.org/10.1016/j.bbabio.2006.11.019.
20. Liu, B., Zhao, F., Zhou, H., et al. (2022). Photoprotection conferring plant tolerance to freezing stress through rescuing photosystem in evergreen Rhododendron. Plant Cell Environ. ***45***(7): 2093–2108. https://doi.org/10.1111/pce.14322.
21. Hormaetxe, K., Hernández, A., Becerril, J.M., et al. (2004). Role of red carotenoids in photoprotection during winter acclimation in Buxus sempervirens leaves. Plant Biol. ***6***(03): 325–332. https://doi.org/10.1055/s-2004-817883.

22. Mbow, H., Reisinger, A., Canadell, J., et al. (2017). Special Report on climate change, desertification, land degradation, sustainable land management, food security, and greenhouse gas fluxes in terrestrial ecosystems (SR2). Ginevra, IPCC ***650***.
23. Yamazaki, J.y., Ohashi, A., Hashimoto, Y., et al. (2003). Effects of high light and low temperature during harsh winter on needle photodamage of Abies mariesii growing at the forest limit on Mt. Norikura in Central Japan. Plant Sci. ***165***(1): 257–264. https://doi.org/10.1016/S0168-9452(03)00169-9.
24. Hughes, N.M. (2011). Winter leaf reddening in 'evergreen' species. New Phytol. ***190***(3): 573–581. https://doi.org/10.1111/j.1469-8137.2011.03662.x.
25. Yu, Z.C., Zheng, X.T., and Peng, C.L. (2020). Different photoprotection strategies for mid-and late-successional dominant tree species in a high-light environment in summer. Environ. Exp. Bot. ***171***: 103927. https://doi.org/10.1016/j.envexpbot.2019.103927.
26. Zeng, Y., Hao, D., Huete, A., et al. (2022). Optical vegetation indices for monitoring terrestrial ecosystems globally. Nat. Rev. Earth Environ. ***3***(7): 477–493. https://doi.org/10.1038/s43017-022-00298-5.
27. Pastorello, G., Trotta, C., Canfora, E., et al. (2020). The FLUXNET2015 dataset and the ONEFlux processing pipeline for eddy covariance data. Sci. Data ***7***(1): 225. https://doi.org/10.1038/s41597-020-0534-3.
28. Howell, T., Meek, D., and Hatfield, J. (1983). Relationship of photosynthetically active radiation to shortwave radiation in the San Joaquin Valley. J. Agric. Meteorol. ***28***(2): 157–175. https://doi.org/10.1016/0002-1571(83)90005-5.
29. Sahaf, M., and Sharon, E. (2016). The rheology of a growing leaf, stress-induced changes in the mechanical properties of leaves. J. Exp. Bot. ***67***(18): 5509–5515. https://doi.org/10.1093/jxb/erw316.
30. Hikosaka, K., Ishikawa, K., Borjigidai, A., et al. (2006). Temperature acclimation of photosynthesis: mechanisms involved in the changes in temperature dependence of photosynthetic rate. J. Exp. Bot. ***57***(2): 291–302. https://doi.org/10.1093/jxb/erj049.
31. Luo, X., Zhou, H., Satriawan, T.W., et al. (2024). Mapping the global distribution of C4 vegetation using observations and optimality theory. Nat. Commun. ***15***(1): 1219. https://doi.org/10.1038/s41467-024-45606-3.
32. Hartmann, D. (1994). The Global Energy Balance. Int. Geophys. ***56***: 18–39.
33. Treharne, R., Bjerke, J.W., Tømmervik, H., et al. (2019). Arctic browning, Impacts of extreme climatic events on heathland ecosystem CO_2 fluxes. Global Change Biol. ***25***(2): 489–503. https://doi.org/10.1111/gcb.14500.
34. Liu, L., Gudmundsson, L., Hauser, M., et al. (2020). Soil moisture dominates dryness stress on ecosystem production globally. Nat. Commun. ***11***(1): 4892. https://doi.org/10.1038/s41467-020-18631-1.
35. Fernández-Marín, B., Gulías, J., Figueroa, C.,I., et al. (2020). How do vascular plants perform photosynthesis in extreme environments? An integrative ecophysiological and biochemical story. Plant J. ***101***(4): 979–1000. https://doi.org/10.1111/tpj.14694.
36. Sun, J., Liu, W., Pan, Q., et al. (2022). Positive legacies of severe droughts in the Inner Mongolia grassland. Sci. Adv. ***8***(47): eadd6249. https://doi.org/10.1126/sciadv.add6249.
37. Renkova, A.G., Khabibrakhmanova, V.R., Gurjanov, O.P., et al. (2023). Changes in the Content of Carotenoids in Moss Shoots Hylocomium splendens Hedw. under Conditions of Temperature Stress. Russ. J. Plant Physiol. ***70***(7): 178. https://doi.org/10.1134/S1021443723603117.
38. Solhaug, K., and Gauslaa, Y. (2011). Secondary Lichen Compounds as Protection against Excess Solar Radiation and Herbivores. Progress in Botany. ***73*** (Springer Press), pp. 289–304.
39. Abdi, H. (2003). Partial Least Square Regression (PLS Regression). Encyclopedia for Research Methods for the Social Sciences (SAGE Publications), pp. 792–795. https://doi.org/10.1007/978-1-4419-9863-7_1274.
40. Wang, F., Harindintwali, J.-D., Wei, K., et al. (2023). Climate change: Strategies for mitigation and adaptation. Innovation Geosci. ***1***(1): 100015. https://doi.org/10.59717/j.xinn-geo.2023.100015.
41. Li, X., Mauzerall, D.L., and Bergin, M.H. (2020). Global reduction of solar power generation efficiency due to aerosols and panel soiling. Nat. Sustain. ***3***(9): 720–727. https://doi.org/10.1038/s41893-020-0553-2.
42. Rantanen, M., Karpechko, A.Y., Lipponen, A., et al. (2022). The Arctic has warmed nearly four times faster than the globe since 1979. Commun. Earth Environ. ***3***(1): 168. https://doi.org/10.1038/s43247-022-00498-3.
43. Short, A., Fay, T.P., Crisanto, T., et al. (2023). Kinetics of the xanthophyll cycle and its role in photoprotective memory and response. Nat. Commun. ***14***(1): 6621. https://doi.org/10.1038/s41467-023-42281-8.
44. Gamon, J.A., Huemmrich, K.F., Wong, C.Y.S., et al. (2016). A remotely sensed pigment index reveals photosynthetic phenology in evergreen conifers. Proc. Natl. Acad. Sci. USA ***113***(46): 13087–13092. https://doi.org/10.1073/pnas.1606162113.
45. Féret, J.B., Gitelson, A., Noble, S., et al. (2017). PROSPECT-D: Towards modeling leaf optical properties through a complete lifecycle. Remote Sens. Environ. ***193***: 204–215. https://doi.org/10.1016/j.rse.2017.03.004.
46. Vermote, E., and Wolfe, R. (2015). In MODOCGA MODIS/Terra Ocean Reflectance Daily L2G-Lite Global 1km SIN Grid V006 (NASA EOSDIS Land Processes Distributed Active Archive Center).
47. Vermote, E., and Wolfe, R. (2015). MYDOCGA MODIS/Aqua Ocean Reflectance Daily L2G-Lite Global 1km SIN Grid V006. In NASA EOSDIS Land Processes DAAC.
48. Myneni, R., Knyazikhin, Y., and Taejin, P. (2015). - MYD15A2H MODIS/Aqua Leaf Area Index/FPAR 8-Day L4 Global 500m SIN Grid. In NASA EOSDIS Land Processes DAAC.
49. Huang, M., Piao, S., Ciais, P., et al. (2019). Air temperature optima of vegetation productivity across global biomes. Nat. Ecol. Evol. ***3***(5): 772–779. https://doi.org/10.1038/s41559-019-0838-x.
50. Rodell, M., Houser, P.R., Jambor, U., et al. (2004). The global land data assimilation system. Bull. Am. Meteorol. Soc. ***85***(3): 381–394. https://doi.org/10.1175/BAMS-85-3-381.
51. Eyring, V., Bony, S., Meehl, G.A., et al. (2016). Overview of the Coupled Model Intercomparison Project Phase 6 (CMIP6) experimental design and organization. Geosci. Model Dev. (GMD) ***9***(5): 1937–1958. https://doi.org/10.5194/gmd-9-1937-2016.
52. Cook, B.I., Mankin, J.S., Marvel, K., et al. (2020). Twenty-first century drought projections in the CMIP6 forcing scenarios. Earth's Future ***8***(6): e2019EF001461. https://doi.org/10.1029/2019EF001461.
53. Loveland, B. (1995). The IGBP-DIS 1 km land cover project. In The 21st Annual Conference of the Remote Sensing Society, P. Curran and Y. Robertson, eds. (Southampton, Univerity of Southampton), pp. 1099–1106.
54. Olson, D.M., Dinerstein, E., Wikramanayake, E.D., et al. (2001). Terrestrial Ecoregions of the World: A New Map of Life on Earth. Bioscience ***51***(11): 933–938. https://doi.org/10.1641/0006-3568(2001)051[0933:TEOTWA]2.0.CO;2.
55. Körner, C., Möhl, P., and Hiltbrunner, E. (2023). Four ways to define the growing season. Ecol. Lett. ***26***(8): 1277–1292. https://doi.org/10.1111/ele.14260.
56. Schafer, R. (2011). What is a Savitzky-Golay filter? IEEE Signal Process. Mag. ***28***(4): 111–117. https://doi.org/10.1109/MSP.2011.941097.
57. Cheng, F., Wang, X., and Barsky, B. (2001). Quadratic B-spline curve interpolation. Comput. Math. Appl. ***41***(1-2): 39–50. https://doi.org/10.1016/S0898-1221(01)85004-5.

ACKNOWLEDGMENTS

This work used eddy covariance data acquired and shared by the FLUXNET community. The *in situ* foliar reflectance dataset was provided by Alexei Solovchenko. The aerial hyperspectral data of canopy reflectance were provided by Kelsey Huelsman. The research was cofunded by the Innovative Research Program of the International Research Center of Big Data for Sustainable Development Goals (CBAS2022IRP03), the National Science Foundation of China (42276241), and the International Joint Research Project of Chinese Academy of Sciences (183611KYSB20200059).

AUTHOR CONTRIBUTIONS

Conceptualization, W.W., X.L., and H.G.; methodology and analysis, W.W., X.X., and J.L.; writing, W.W., H.E., and X.X.

DECLARATION OF INTERESTS

The authors declare no competing interests.

SUPPLEMENTAL INFORMATION

It can be found online at https://doi.org/10.1016/j.xinn.2024.100649.

LEAD CONTACT WEBSITE

https://www.webofscience.com/wos/author/record/2082620.